nature COMMUNICATIONS

REVIEW ARTICLE

https://doi.org/10.1038/s41467-022-28723-9 OPEN

Self-healing oxygen evolution catalysts

Agnes E. Thorarinsdottir [1,2], Samuel S. Veroneau [1,2] & Daniel G. Nocera [1✉]

Electrochemical and photoelectrochemical water splitting offers a scalable approach to producing hydrogen from renewable sources for sustainable energy storage. Depending on the applications, oxygen evolution catalysts (OECs) may perform water splitting under a variety of conditions. However, low stability and/or activity present challenges to the design of OECs, prompting the design of self-healing OECs composed of earth-abundant first-row transition metal oxides. The concept of self-healing catalysis offers a new tool to be employed in the design of stable and functionally active OECs under operating conditions ranging from acidic to basic solutions and from a variety of water sources.

Large-scale implementation of sustainable energy is needed to address the rising energy demands of our society while avoiding the detrimental impacts of fossil fuels. Whereas sustainable energy supplies (e.g., solar energy) are abundant, their implementation is bottlenecked by the challenge of storing this energy at the scale of societal demand[1–3]. One potentially scalable approach to energy storage is the production of hydrogen gas (H_2) through renewably-driven electrochemical water splitting[1,2,4,5]. Hydrogen is a reliable energy carrier that can be used directly as a green fuel[2], or be employed to furnish increasingly energy-dense products, including liquid fuels[6–9] ammonia[10,11]. Water splitting (Eq. (1)) is an endergonic process that demands an external energy input greater than the thermodynamic minimum of 1.23 V to proceed:

$$2H_2O \rightarrow O_2 + 2H_2 \; E^o = E^o_{HER} - E^o_{OER} = -1.23\,V \quad (1)$$

$$2H_2O \rightarrow O_2 + 4H^+ + 4e^- \; E^o_{OER} = 1.23\,V - 0.059\,V \times pH \quad (2)$$

$$4H^+ + 4e^- \rightarrow 2H_2 \; E^o_{HER} = 0V - 0.059\,V \times pH \quad (3)$$

Thus, renewable energy, whether it be from solar or wind, may be stored in the rearranged bonds of water as H_2 and O_2[1]. Of the two half-reactions of water splitting (Eqs. (2), (3)), the $4e^-/4H^+$ oxygen evolution reaction (OER) is particularly demanding[12]. The most active and stable oxide catalysts for OER comprise critical metals (i.e., Ru, Ir)[13]. However, with regard to commercially relevant applications, they are not stable enough[14,15] and they are costly owing to their scarcity. These challenges provide an imperative for the development of oxygen evolution catalysts (OECs) from earth-abundant elements that are both highly active and stable in various water sources under a range of operating conditions[16–18].

Earth-abundant first-row transition metal oxides, however, have been relegated to operation in concentrated base[13,19]. The presence of base is required because metal oxides are themselves basic according to the Lux classification[20] and will readily react with protons produced through OER (Eq. (2)), leading to damage (i.e., dissolution, corrosion, protonation). In concentrated base, hydroxide (OH^-) is the strongest base and will neutralize these protons to protect the oxide;

[1] Department of Chemistry and Chemical Biology, Harvard University, Cambridge, MA 02138, USA. [2] These authors contributed equally: Agnes E. Thorarinsdottir, Samuel S. Veroneau. ✉email: dnocera@fas.harvard.edu

however, in less basic solutions, the concentration of OH^- is not sufficient making the primary base the oxide itself, leading to catalyst damage and inactivation. The ability to operate in non-basic conditions has advantages of using natural water sources[21], facilitating the interfacing of catalysts with materials such as Si[22–26], which is unstable in corrosive basic conditions, reducing liability associated with technology advancement especially for distributed systems, and enabling the interfacing of water splitting catalysis to bio-organisms in hybrid inorganic–biological devices[8,9,27,28]. A unique strategy for operating earth-abundant first-row transition metal oxide OECs outside of strongly basic conditions is through the implementation of self-healing.

Within the catalysis community, multiple definitions of self-healing and self-repairing catalysts have been proposed[29,30]. The concept of self-healing has historically been used to describe any material with the ability to repair itself. Materials ranging from bio-inspired systems[31,32] to synthetic organic polymers[33–35], inorganic–organic hybrid materials, and metallic systems[36–38] have all been considered self-healing. This can be through autonomous or stimuli-triggered processes that occur without or with external input (e.g., energy, pressure, chemical healing agents), respectively[34–38]. Many materials described as self-healing, including bio-inspired synthetic materials and metallic systems, however, induce repair after significant functional damage has already occurred, involve processes outside of normal operation, or rely upon the presence of chemical healing agents that are continually depleted[34–38]. We restrict the term "self-healing" herein to describe systems that continually regenerate themselves through a dynamic equilibrium during catalysis and under a given set of operating conditions. For example, self-healing notably differs from the repair mechanism of the Oxygen-Evolving Complex in Photosystem II, where the damaged reaction center is continuously replaced by a newly synthesized copy[39,40]. Furthermore, based on our criteria, catalyst regeneration mechanisms that rely on chemical oxidants (e.g., Ce^{4+})[41], require activation by light to release oxygen and regenerate the precatalytic resting state[42], or involve regeneration at conditions outside of that required for catalysis[43] are considered self-repairing but not self-healing. Self-repairing metal oxide-based OECs have been comprehensively reviewed[44].

Figure 1 schematically contrasts OECs that degrade with ones that self-repair and self-heal. Electrochemical and photoelectrochemical OER relies upon applying an external bias (potential) to the OEC to promote reactivity (Eq. (2)). Self-healing OECs are realized when this external bias is sufficient to drive regeneration such that the rate of repair is greater than or equal to the rate of damage. The required potential for this process is therefore less than or equal to the potential required to drive OER (Fig. 1C). This requirement is not fulfilled by self-repairing OECs, thus distinguishing self-healing from self-repairing catalysts. This is illustrated schematically in Fig. 1B where metal ions at equilibrium in solution can (re)deposit onto the still active and functional catalyst, assuming adequate mass transport from the solution to the electrode surface[30]. At equilibrium, it may be considered that there is no net degradation of catalyst, to reconcile a previous definition of self-healing[29]. We emphasize that self-healing as defined here *is not established universally by structure/composition but rather is defined operationally*. For oxide catalysts, structural and compositional damage occurs most commonly by protonation of surface oxo-species and the subsequent amorphization or dissolution of surface metal species; degradation mechanisms of OECs may also involve other structural rearrangement, mechanical, and poisoning effects[45]. The ability of the catalyst to regenerate itself will depend on the types and amounts of electrolytes and buffers, bulk pH values, applied currents and potentials, temperature, mass transport conditions, etc. Consequently, a homogeneous or heterogeneous OER catalyst of a given composition, crystallinity, or polymorphism may degrade under one set of conditions and not another. Thus, self-healing is determined by the set of conditions in which the catalyst operates.

We now survey the current state of OECs based on first-row transition metal oxides that exhibit self-healing behavior. Dimensional reduction of first-row metal oxides of Mn, Co, and Ni gives rise to metallate oxygen evolution catalysts (M-OECs) that exhibit high activity for OER[46–49]. We focus on the kinetics of OER and self-assembly, which form the foundation for the inherent self-healing properties of M-OECs. We highlight how the distinct kinetics of these processes determine the stability and activity of catalysts under different operating conditions, how the concept of self-healing is extended to multimetallic systems and discuss future approaches to developing increasingly active self-healing OECs.

Self-healing Co-OECs

Cobalt-based M-OECs (Co-OECs) in the presence of phosphate (P_i) and borate (B_i) are exemplar self-healing OECs (Co-OECs generated in the presence of P_i or B_i are referred to hereafter as CoP_i and CoB_i, respectively). These catalysts are generated as amorphous thin films on various conductive substrates (e.g., indium tin oxide, fluorine-doped tin oxide) during anodic electrodeposition from dilute aqueous Co^{2+} solutions in the presence of P_i[50], methylphosphonate (MeP_i)[51], or B_i[21,52] electrolytes in neutral to mildly basic conditions. These oxoanions facilitate the dimensional reduction of extended metal oxides by capping cluster growth to give rise to metallate active sites, which range from 10 to 60 metal centers, as deduced from X-ray pair distribution function (PDF) analysis of heterogeneous films[52–55]. The molecular nature of the M-OECs has allowed the mechanism of OER catalysis to be defined at a molecular and atomistic level. Isotopic measurements using differential electrochemical mass spectrometry[56] together with electrokinetics[51], spectroscopic[57], and computational[58,59] studies establish that O–O bond formation occurs by proton-coupled electron transfer (PCET) at cobaltate cluster edge sites.

Figure 2A shows the mechanism for OER catalyzed by Co-OECs. The catalyst resides in a $Co^{III}Co^{III}$ resting state (vide infra), as highlighted in Fig. 2B, from which the $Co^{III}Co^{IV}$ precatalytic state is generated. Here, the terminal Co^{IV}–oxo (i.e., $Co^{IV}=O$) is better formulated as a Co^{III}–oxyl (i.e., Co^{III}–O•) radical based on the electronic considerations embodied by the "oxo wall"[60]. Tafel analysis at pH 7 reveals a slope of 59 mV dec^{-1}, indicating that the active $Co^{IV}Co^{IV}$ catalyst is generated by a $1e^-/1H^+$ pre-equilibrium step followed by a turnover rate-limiting chemical step involving O–O bond formation and O_2 release[61]. Accordingly, the rate of OER possesses an inverse first-order dependence of $\log(j_{OER})$ on proton activity (i.e., first-order dependence on pH), as summarized in the following electrochemical rate law obtained from electrokinetics studies:

$$j_{OER} = k_0^{OER}(a_{H+})^{-1}\exp(FE/RT) \quad (4)$$

where j_{OER} is the current density for OER and k_0^{OER} is a potential-independent constant that is proportional to the exchange current density for OER.

Self-healing is established between the interplay of the potential required for OER and that required for self-assembly (i.e., deposition and regeneration) of the Co-OECs. Electrochemical kinetics have revealed the mechanism for catalyst deposition/regeneration to be as shown in Fig. 2B. At the deposition potential of 1.0 V vs. the normal hydrogen electrode (NHE) there is a minor Nernstian population of Co^{4+}, as verified by EPR spectra of CoP_i films[62], and consistent with the redox Co^{3+}/Co^{4+} midpotential[63]. The Co^{4+} on the electrode oxidizes Co^{2+} in

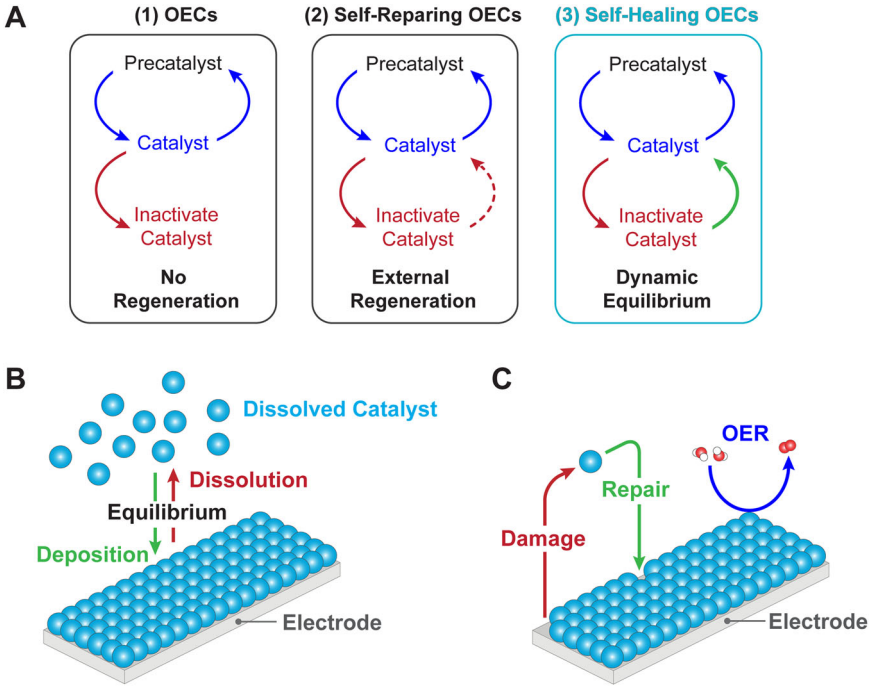

Fig. 1 Schematic depiction of self-healing OECs. A Self-repairing OECs (center) are a specific type of OECs (left) that may operate for a prolonged time as they are regenerated once they become inactive, usually with the aid of an external input (e.g., energy, pressure, chemical healing agents). Self-healing OECs (right) are a specific type of OECs that continually regenerate themselves through an equilibrium process that occurs under the operating conditions of OER. **B** Graphical representation of the competing effects of catalyst deposition and dissolution that give rise to the equilibrium implicit for self-healing OECs. **C** Based on the equilibrium shown in (**B**), a damaged site is continuously repaired during OER for self-healing OECs, and as the rate of repair is greater than or equal to the rate of damage, no loss of catalytic species is observed. Blue spheres represent a catalytically competent metal capable of self-healing (e.g., Mn, Co, Ni, Cu).

solution, which is in the form of $Co(OH)(OH_2)_5^{+}$ at the 1.0 V deposition potential, by inner-sphere electron transfer upon dissociation of P_i, giving rise to substitutionally inert Co^{3+} that adds to the exposed edge sites for metallate cluster growth. The pH dependence of CoP_i film deposition reveals an inverse third-order dependence on proton activity (i.e., third-order dependence of $\log(j_{OER})$ on pH), as well as an inverse first-order dependence on $[P_i]$, and first-order dependence on $[Co^{2+}]$, owing to the need to dissociate P_i for the inner-sphere electron transfer between Co^{4+} on the surface and $Co(OH)(OH_2)_5^{+}$ in solution[64]. Thus, the overall rate law for deposition of CoP_i is[65]:

$$j_{dep} = k_0^{dep}[Co^{2+}](a_{H+})^{-3}[P_i]^{-1}\exp(FE/RT) \quad (5)$$

where j_{dep} is the current density for catalyst deposition/regeneration and $k_0{}^{dep}$ is a potential-independent constant that is proportional to the exchange current density for the deposition/regeneration process.

Self-healing is achieved because the potential needed to drive CoP_i film self-assembly (i.e., produce Co^{4+} for deposition) occurs at 0.2 V below the potential required for sustaining OER. Accordingly, potentials sufficient to sustain OER will oxidize any Co^{2+} in solution that may have leached from the film during operation and, thus, induce instantaneous redeposition. The transport of Co^{4+} in CoP_i films (i.e., the oxidizing hole equivalent) is predicted to be fast based on the $Co^{3+/4+}$ self-exchange electron transfer rate constant of $k_{ET}(Co^{3+/4+}) = 3 \times 10^5\ M^{-1}\ s^{-1}$ as measured in cobalt cubane model complexes[66]. Because such hole hopping through the film is fast relative to Co^{2+} deposition[62,67], very little Co^{2+} is produced in solution. Nonetheless, as confirmed by Co-57 radiolabeling of CoP_i films, any Co^{2+} released in solution is redeposited via the mechanism shown in Fig. 2B[68]. Consequently, no film dissolution is observed during OER when P_i is present at intermediate-to-high concentration (>~1 mM). Furthermore, this self-healing mechanism also applies for Co-OECs with MeP_i and B_i oxoanions, and similar self-healing Co-OECs are posited to form from the decomposition of molecular cobaloxime precursors in B_i buffer solutions (pH 9.2) upon application of high positive potentials[69].

The disparate pH profiles for OER and catalyst generation for Co-OECs give rise to a "Pourbaix" diagram for self-healing. Because of the steeper inverse third-order dependence on proton activity for deposition, the potential necessary for catalyst self-assembly rises much more rapidly with decreasing pH as compared to that for OER. As highlighted by the teal zone in Fig. 3A, the potentials necessary to sustain catalyst film formation are well below those required for OER. Thus, as long as Co-OECs are operated in the teal zone in Fig. 3A (pH > 5.2) the catalysts are indefinitely stable in aqueous solutions under the operational conditions that promote self-healing. This functional stability range for CoP_i is further supported by the observation of catalyst damage at pH 5 and below[47,65]. By introducing 0.1–1 mM Co^{2+} to the buffered electrolyte, however, Co-OECs may remain functionally stable down to pH of ~3 as the increased concentration of Co^{2+} drives a dynamic equilibrium, as shown in Fig. 2B, toward catalyst deposition and thus regeneration[70,71]. Below pH ~3, however, these low concentrations of Co^{2+} are insufficient to offset metal oxide dissolution and catalyst damage cannot be reversed. Notably, operational stability of Co-OECs at pH 1.6 can be achieved at higher Co^{2+} concentrations of 0.6 M in phosphate or sulfate electrolytes under application of potentials above 2.05 V vs. NHE[72].

The CoP_i OER catalyst is exemplary of the concept of self-healing from an operational as opposed to a structural or compositional viewpoint. As emphasized for CoP_i, self-healing is not achieved when the buffer concentration is too low[29,71], as the rate

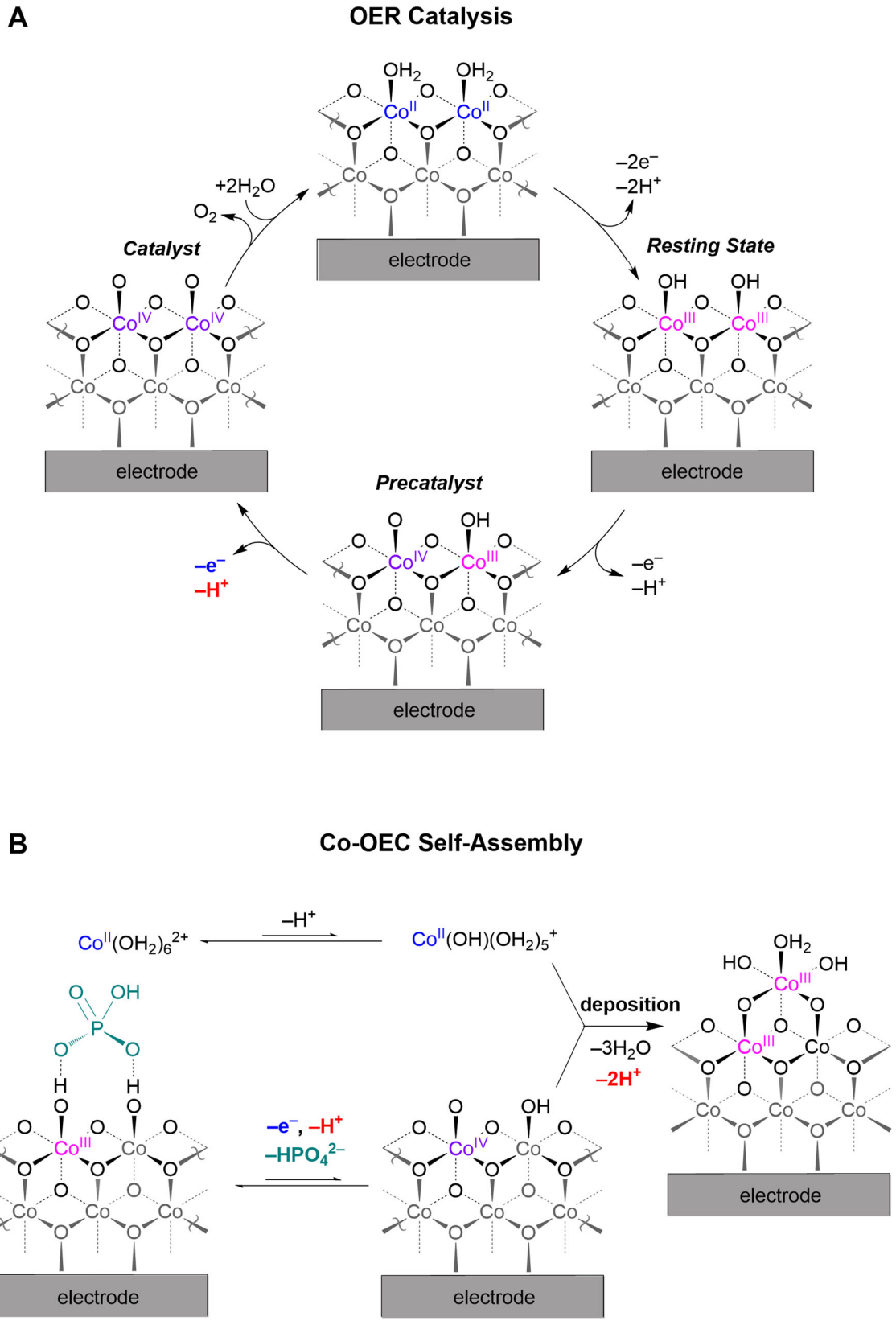

Fig. 2 Co-OEC catalysis and self-assembly. A Proposed OER catalytic cycle (top cycle in Fig. 1A (3)) for Co-OECs (i.e., CoP_i, $CoMeP_i$, CoB_i), as determined from spectroscopic analysis and electrochemical kinetics studies for CoP_i. **B** Proposed mechanism for the generation of Co-OEC films (bottom cycle in Fig. 1A (3), and green arrows in Fig. 1B, C). The protons (H^+) that appear in the electrochemical rate laws for OER and catalyst deposition/ regeneration are highlighted in red.

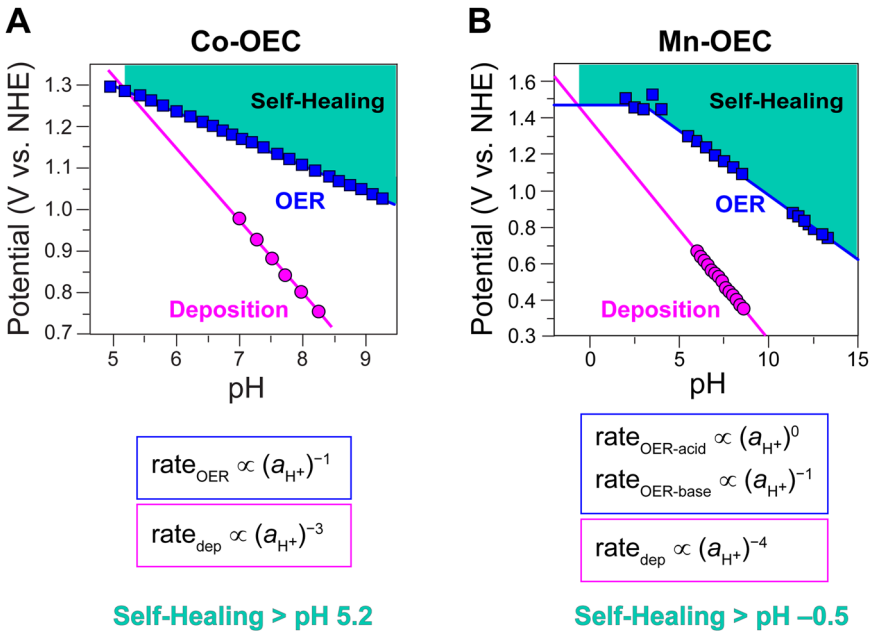

Fig. 3 Pourbaix diagrams for Co- and Mn-OECs. Potential–pH diagrams for (**A**) Co-OECs and (**B**) Mn-OECs at fixed current densities of $j = 30$ and 1.3 μA cm^{-2} (based on geometric electrode surface area), respectively. The dependence of the rate of OER and the rate of catalyst deposition/regeneration on proton activity (a_{H+}) are highlighted in blue and magenta, respectively, for each catalyst type. The different pH dependence for the two processes forms the foundation for the self-healing properties of Co-OECs and Mn-OECs above pH 5.2 and −0.5, respectively, in solutions devoid of component metals as indicated with the teal zones in the graphs. All potentials are referenced to the NHE scale.

of catalyst redeposition is smaller than the rate of dissolution. Hence under one set of conditions (e.g., low P_i concentration or a given current, potential, etc.) CoP_i is self-repairing, while under a different set of conditions that establishes Fig. 1C, CoP_i is self-healing. As a metric, a self-healing catalyst under operating conditions has a turnover number that is extremely large and in the limit approaches infinity.

Self-healing Mn-OECs

Modulating the relationship between potential and pH for OER and self-assembly can lead to extraordinary catalytic properties. Self-healing in a Mn-OEC produced by electrodeposition from dilute Mn^{2+} solutions in a weakly basic electrolyte furnishes a stable OER catalyst at pHs as low as –0.5[73–75]. The rate of OER by Mn-OECs in P_i and MeP_i electrolytes is zeroth order in proton activity at pH < 3.5 and inverse first order in proton activity at pH > 3.5. Based on Tafel analysis, two parallel OER mechanisms shown in Fig. 4A have been proposed in these different pH regions: (1) a Mn^{3+} disproportionation process with zeroth-order dependence on proton activity that predominates at pH < 3.5 and (2) a $1e^-/1H^+$ pathway that is dominant at pH > 3.5. This modest pH dependence for OER is juxtaposed to a significant pH dependence for deposition. An inverse fourth-order dependence on proton activity arises from a turnover-limiting disproportionation reaction, which also gives rise to a second-order dependence on Mn^{2+} concentration[73]. This steep pH dependence for catalyst deposition results in a potential–pH diagram with a crossing for OER and catalyst deposition/regeneration at pH –0.5 (Fig. 3B), allowing the Mn-OEC to operate in concentrated acid. The functional stability of Mn-OECs is supported by ^{31}P NMR line width analysis when using MeP_i as an electrolyte[74]. The stability of Mn-OECs, however, is complicated by the formation of MnO_4^- ions at high potentials, preventing operation at high current densities (and attendant higher potentials) for OER[76]. As such, the stability of Mn-OECs in acidic electrolytes is maintained only at low OER current densities (< 1 mA cm^{-2}). Activation of Mn-OECs by potential cycling affords a substantial improvement in OER activity, resulting in two orders of magnitude increase in current density at pH 2.5[73]. This activity enhancement for Mn-OECs upon varying the synthesis protocol[73,77] suggests that the generation of acid-stable Mn-OECs that show higher OER activity is possible.

Self-healing Ni-OECs

Self-healing Ni-OEC may be established with B_i as the electrolyte, as P_i is unable to support nickelate cluster formation[78–80]. The NiB_i catalyst is prepared by anodic electrodeposition from dilute aqueous Ni^{2+} solutions in the presence of B_i at pH 9.2. Subsequent activation by anodization affords enhanced OER activity owing to an average increase in the Ni oxidation state from +3.2 to +3.6, indicating substantial generation of formally Ni^{4+} species, whereas non-activated films are predominately Ni^{3+}[79,80]. The mechanism for NiB_i self-healing resembles that of CoP_i with the caveat that Tafel analysis of NiB_i furnishes an OER rate law that is inverse first order in [B_i] (i.e., for 20–300 mM B_i) and inverse third order in proton activity (i.e., for pH 8.5–12). The $2e^-/3H^+$ pre-equilibrium followed by a rate-limiting O–O bond formation and O_2 release is shown in Fig. 5. Despite the ostensible "inhibitory" effect of B_i on OER kinetics, the activity of NiB_i is high owing to the differences of B_i vs. P_i substitution. Whereas P_i must exchange at dicobalt edge sites by a dissociative substitution mechanism, B_i can exchange with more facility at edge sites via Lewis acid–base mechanism[56].

The differences in the role of electrolyte between Co-OECs and Ni-OECs highlight the pivotal role that electrolytes play in OER and self-healing by facilitating proton transfer at intermediate pHs and by establishing the equilibrium for catalyst deposition/regeneration. The different characteristics of the PCET pre-equilibrium (and thus Tafel slope) for CoP_i and NiB_i and associated disparate pH dependences for these catalysts render NiB_i increasingly more active than CoP_i as the pH is elevated. However, CoP_i outperforms NiB_i at

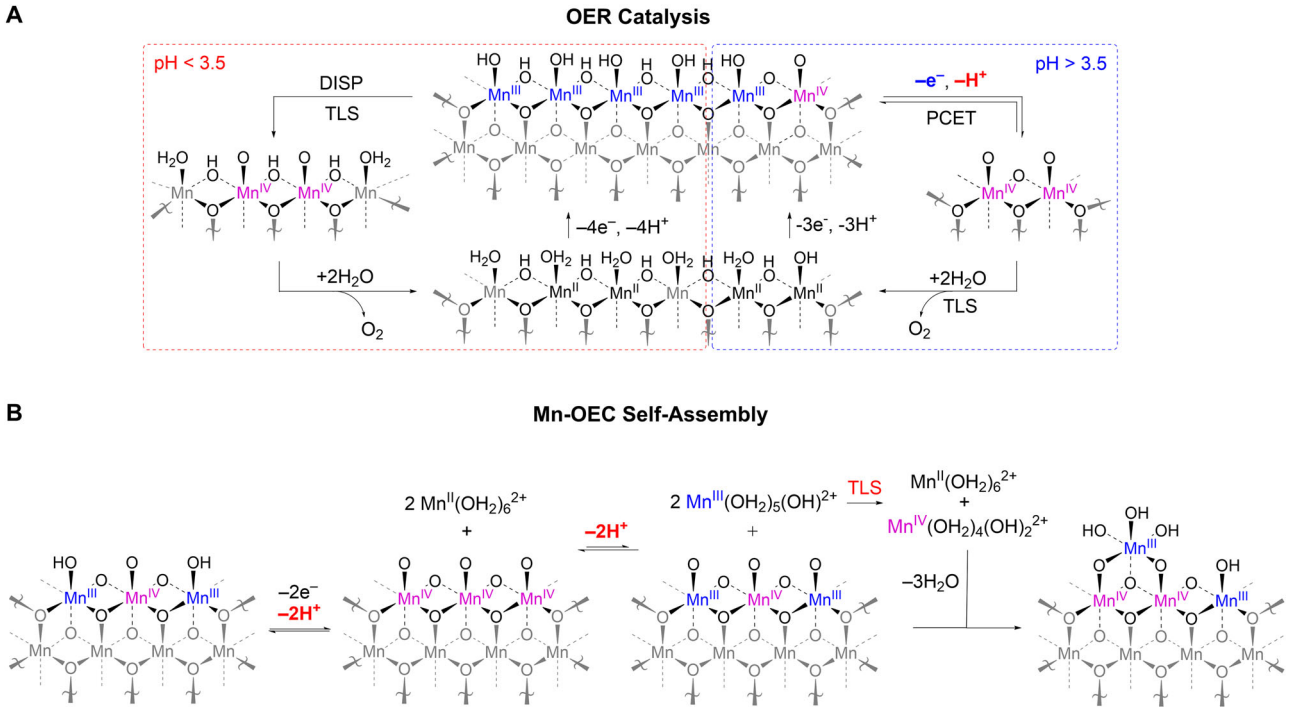

Fig. 4 Mn-OEC catalysis and self-assembly. A Proposed OER catalytic cycle for Mn-OECs, as determined from spectroscopic analysis and electrochemical kinetics studies at different pHs. **B** Proposed mechanism for the generation of Mn-OEC films. The protons (H^+) that appear in the electrochemical rate laws for OER and catalyst deposition/regeneration are highlighted in red. Owing to the disproportionation reaction involving two manganese complexes, an inverse fourth-order proton dependence is observed, enabling self-healing to be preserved at pH > ~0.5. DISP and TLS denote disproportionation and turnover-limiting step, respectively.

neutral and slightly acidic conditions[79]. On that note, Ni-OECs are not stable in acidic electrolytes at moderate overpotentials owing to dissolution of the oxides, as judged by the Pourbaix diagram of Ni in water[76]. In contrast, Ni-OECs are stable at alkaline pHs and display self-healing in concentrated base (e.g., 0.1–1.0 M KOH) devoid of buffer electrolytes[79]. Accordingly, Ni-OECs exhibit self-healing properties at pH ~9–14, however, the pH dependence of the Ni-OEC film assembly process remains to be defined to enable the construction of potential-pH diagrams such as those shown for Co-OECs and Mn-OECs in Fig. 3.

As with Co-OECs, catalytically active Ni-OEC films may form from molecular complexes that provide the requisite metal ions[81]. The use of a proton-accepting B_i electrolyte has been shown to be necessary to achieve and maintain high catalytic activity for these Ni-OECs at pH 9.2. The facility with which M-OEC films form from molecular complexes highlights the difficulties associated with deploying molecular systems as OER catalysts. Specifically, determining whether catalytic activity is derived from the initial molecular species or from the generation of small amounts of M-OECs, where the molecular complex serves as a metal source, remains a challenging task.

Self-healing in Cu-OECs

Self-healing has been imparted to Cu-OECs where sustained OER is achieved in a carbonate buffer (pH ~ 10.8) containing sufficient dissolved Cu^{2+} to drive catalyst self-assembly[82]. Here, formation of a compact film of CuO on a Cu surface prevents anodic corrosion and enables sustained OER catalysis.

Self-healing mixed-metal OECs

Mixed-metal oxide OECs with catalytic and structural metals. Self-healing may be augmented by alloying catalytically active metal elements with structural metal elements to further enhance stability. In a common class of mixed-metal oxide OECs (M′M–OECs), some components may themselves be formally self-healing while other components function predominantly as structural elements (Fig. 6A) such that OER activity and stability are decoupled and therefore may be optimized independently[83]. The incorporation of various catalytically active metals into a shared inert oxide framework can fortify the metal–oxygen bonds that are generally weakened during OER, particularly at active sites, leading to enhanced stability while preserving high OER activity. Among the most common types of M′M–OECs are systems where a catalytically competent metal (e.g., Mn, Fe, Co, Ni) is doped into a conductive and thermodynamically stable matrix (e.g., PbO_x) to achieve materials with simultaneous high activity and stability under acidic conditions[83,84]. For example, the self-healing and structurally fortified $CoFePbO_x$ is functionally stable under optimized reaction conditions (i.e., 5 mM Co^{2+}, 1 mM Fe^{3+}, 0.5 mM Pb^{2+}) at both ambient and elevated temperatures in solutions of pH 0–1 with no loss of activity after even one week of continuous operation[85]. Since catalyst repair and damage, as well as OER, are all kinetically controlled processes, tuning the concentrations of the component metals, along with temperature and pH, appears to be a promising means of imparting self-healing to M′M–OECs.

Mixed-metal oxide OECs with different catalytic metals. Another common type of M′M–OECs is generated by alloying metals to increase the activity of a unary metal oxide that already displays OER activity (Fig. 6B). The introduction of Fe^{3+} into NiB_i and CoP_i has been shown to be especially effective at increasing OER activity[86–91], though the reason for this enhancement continues to be explored[92]. As Fe-based OECs are not self-healing[93], NiFe-OECs and CoFe-OECs incur a significant loss in stability owing to oxide dissolution under varying conditions[83,84]. Notwithstanding, a dynamically stable CoFe-OEC may be prepared using a nanorod

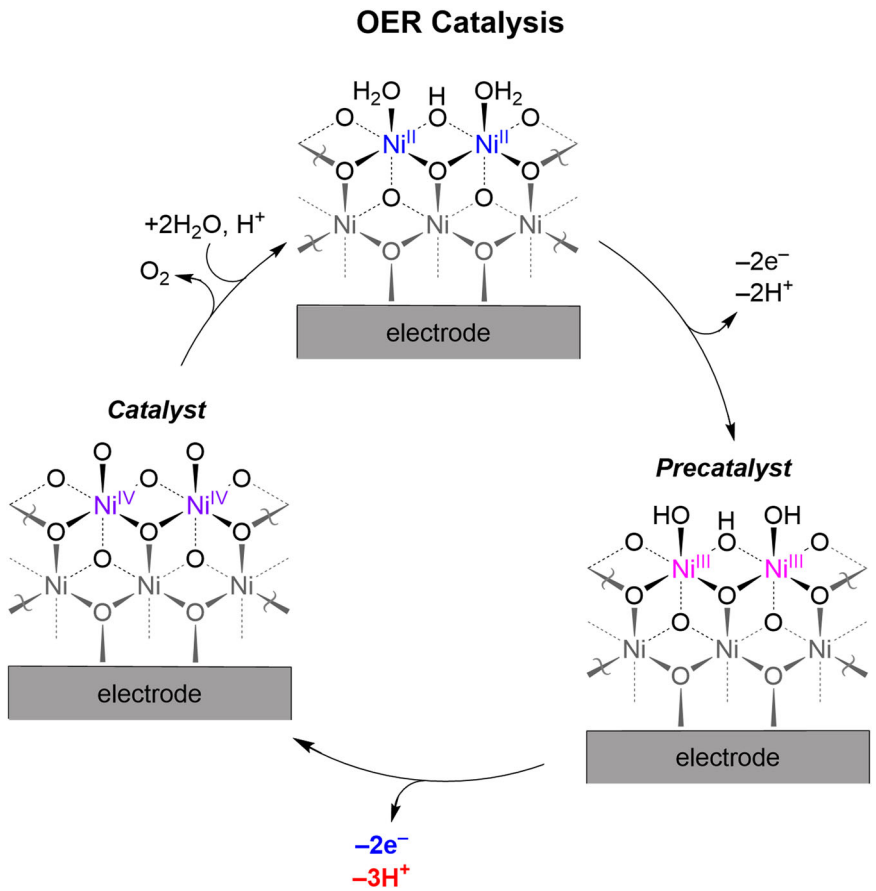

Fig. 5 Ni-OEC catalytic cycle. Proposed OER catalytic cycle for Ni-OEC with B_i as an electrolyte, as determined from spectroscopic analysis and electrochemical kinetics studies for NiB_i.

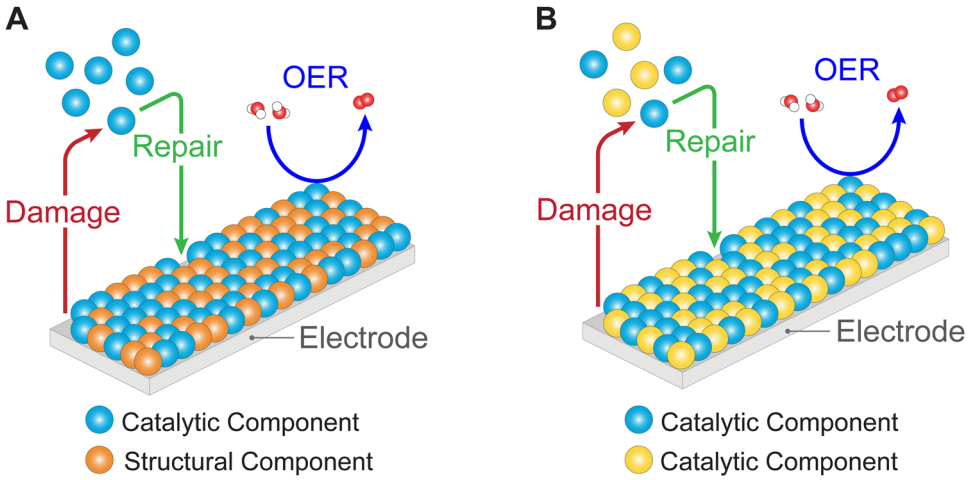

Fig. 6 Schematic depiction of two common types of mixed-metal oxide OECs (M′M-OECs) that may possess self-healing properties. A Self-healing M′M-OEC system composed of separate catalytic (e.g., Co, Ni; blue spheres) and structural components (e.g., PbO_x; orange spheres). **B** Self-healing M′M-OEC system comprising two types of catalytic components (blue, yellow spheres). Self-healing in both types of systems involves the catalytic component(s) undergoing damage and repair while performing OER. The colored spheres above the electrode surface denote dissolved catalyst capable of repair.

array of $CoMoO_4$ as a host matrix for the redeposition of FeOOH and CoOOH in alkaline media[94]. The resulting CoFe-OEC exhibits high OER activity, sustaining an OER current density of 100 mA cm^{-2} (based on geometric electrode surface area) with an overpotential of 298 mV in 1 M KOH. Furthermore, recent work has demonstrated that self-healing may also be achieved by operating in alkaline electrolytes containing a small amount of Fe[95,96]. For example, addition of 0.1 ppm Fe to the operating KOH electrolyte solution was shown to promote self-healing in a range of first-row transition metal oxyhydroxides by facilitating dynamic Fe exchange[95]. Isotopic labeling experiments with ^{56}Fe and ^{57}Fe revealed rapid exchange of isotopes while preserving overall

Fe content, indicating a fast rate of Fe regeneration as compared to the rate of dissolution. Consequently, the electrolyte must contain a sufficiently high concentration of Fe so as to raise the rate of Fe regeneration to engender a high number of dynamic active sites, and thus preserve high OER activity and functional stability. In a related study, introduction of Co into NiFe-OECs was shown to promote redeposition of Fe in situ and, thus, engender catalyst self-healing when operating in strongly alkaline (pH 14) electrolytes containing both ferrous and borate ions[96]. Here, the Fe ions could only be redeposited on sites adjacent to Co sites, preventing the deposition of thick Fe oxyhydroxide overlayers. This unique self-limiting thickness was demonstrated to be ideal for integration with photoelectrodes as a high light transmittance through the catalyst layer could be maintained during OER operation. A similar approach has been taken with NiFe-OECs in carbonate buffer, where long-term stability and self-healing was induced by adding Ni^{2+} and Fe^{3+} to the operating electrolyte in weakly to strongly basic solutions[97]. Together these examples highlight that the competing rates of metal oxide repair and damage may be influenced by tuning the concentrations of dissolved component metals in solution.

Other mixed-metal oxide OECs. Self-healing M′M-OECs beyond typical electrodeposited metal oxide films have also been reported. A NiFe-OEC generated in situ on a Mo-doped $BiVO_4$/Ni/Sn photoelectrode is self-healing in a site-specific manner when operated in a B_i electrolyte by using a passivated Ni contact layer as the source of Ni^{2+}[98]. Similarly, dynamic cycling of dissolution, diffusion, and deposition of Ni and Fe in a Si-based photoanode coated with a dual layer electrocatalyst engenders extended electrode stability[99]. Furthermore, a nanoparticle-based system composed of NiFe-layered double hydroxide nanoparticles deposited onto a Ni electrode has been shown to possess self-healing properties in an alkaline electrolyser[100]. This catalyst is generated in situ during electrolysis driven by electrostatic forces; self-healing is induced by operating in an electrolyte containing the component nanoparticles that continually deposit onto the underlying Ni electrode during operation. Along these lines, a ligand-induced self-healing mechanism was recently reported for a Fe-based electrocatalyst operating in strongly alkaline media[101]. These self-healing approaches are analogous to those described above but rely on a component material or a stabilizing ligand, as opposed to a dissolved metal ion, to direct the damage vs. repair equilibrium toward repair.

Finally, self-healing may directly involve oxide lattice sites. For perovskite systems such as $SrCoO_3$[102], self-healing is derived from surface adsorbed H_2O molecules, which dissociate to form reactive oxygen atoms that fill oxygen vacancies on the surface produced during OER. As the formation of such oxide vacancies define catalyst degradation, their depletion accommodates catalyst repair. This system is self-healing as the onset potential required to drive the filling of the oxygen vacancy is lower than the potential at which OER proceeds. A similar oxygen vacancy-based self-healing property has been proposed for TiO_2[103] and α-MnO_2[104] OECs.

Summary and outlook

The need to implement sustainable energy sources on a global scale has promoted H_2 as a potential energy carrier. Electrochemical water splitting provides a scalable route to H_2 production from renewable sources and has prompted the development of OECs to drive the more challenging oxygen evolution half-reaction. In this effort, self-healing OECs based on earth-abundant first-row transition metal oxides have garnered significant attention owing to their ability to drive OER at relatively low overpotentials while remaining stable under various operating conditions. Self-healing unary metal oxide OECs such as MnO_x, CoP_i, and NiB_i provide activity and stability in acidic, neutral, and basic conditions, whereas emerging mixed-metal oxide OECs such as $CoFePbO_x$ and $NiFeO_x$ offer improved activity and/or stability across a similar range of conditions. Under a wide range of operating conditions, OER catalysts may be more easily interfaced with (1) materials for direct conversion of water to oxygen and hydrogen at high efficiency[24–26,105] and (2) biological organisms to perform artificial photosynthesis[8,9]. A better fundamental understanding of damage and repair mechanisms in existing and future systems may expand the self-healing capabilities of OECs to a wider range of conditions and promote self-healing as a general design principle in catalysis development, opening paths to a broad set of future applications. Overall, this review has highlighted the prospects for self-healing first-row transition metal oxides as OECs in water splitting systems. The increasing need to transition away from fossil fuels necessitates further research into self-healing OECs based on earth-abundant elements, expanding the practicality and utility of these versatile chemical platforms.

Received: 29 October 2021; Accepted: 2 February 2022;
Published online: 10 March 2022

References

1. Lewis, N. S. & Nocera, D. G. Powering the planet: chemical challenges in solar energy utilization. *Proc. Natl. Acad. Sci. USA* **103**, 15729–15735 (2006).
2. Cook, T. R. et al. Solar energy supply and storage for the legacy and nonlegacy worlds. *Chem. Rev.* **110**, 6474–6502 (2010).
3. Abbott, D. Keeping the energy debate clean: how do we supply the world's energy needs? *Proc. IEEE* **98**, 42–66 (2010).
4. Nocera, D. G. Chemistry of personalized solar energy. *Inorg. Chem.* **48**, 10001–10017 (2009).
5. Spitler, M. T. et al. Practical challenges in the development of photoelectrochemical solar fuels production. *Sustain. Energy Fuels* **4**, 985–995 (2020).
6. Li, C. W., Ciston, J. & Kanan, M. W. Electroreduction of carbon monoxide to liquid fuel on oxide-derived nanocrystalline copper. *Nature* **508**, 504–507 (2014).
7. Rabinowitz, J. A. & Kanan, M. W. The future of low-temperature carbon dioxide electrolysis depends on solving one basic problem. *Nat. Commun.* **11**, 5231 (2020).
8. Liu, C., Colón, B. C., Ziesack, M., Silver, P. A. & Nocera, D. G. Water splitting–biosynthetic system with CO_2 reduction efficiencies exceeding photosynthesis. *Science* **352**, 1210–1213 (2016).
9. Dogutan, D. K. & Nocera, D. G. Artificial photosynthesis at efficiencies greatly exceeding that of natural photosynthesis. *Acc. Chem. Res.* **52**, 3143–3148 (2019).
10. Andersson, J. & Grönkvist, S. Large-scale storage of hydrogen. *Int. J. Hydrogen Energy* **44**, 11901–11919 (2019).
11. Klerke, A., Christensen, C. H., Nørskov, J. K. & Vegge, T. Ammonia for hydrogen storage: challenges and opportunities. *J. Mater. Chem.* **18**, 2304–2310 (2008).
12. Eisenberg, R. & Gray, H. B. Preface on making oxygen. *Inorg. Chem.* **47**, 1697–1699 (2008).
13. Surendranath, Y. & Nocera, D. G. Oxygen evolution reaction chemistry of oxide-based electrodes. *Prog. Inorg. Chem.* **57**, 505–560 (2011).
14. Kötz, R., Stucki, S., Scherson, D. & Kolb, D. M. In-situ identification of RuO_4 as the corrosion product during oxygen evolution on ruthenium in acid media. *J. Electroanal. Chem. Interfacial Electrochem.* **172**, 211–219 (1984).
15. Reier, T., Oezaslan, M. & Strasser, P. Electrocatalytic oxygen evolution reaction (OER) on Ru, Ir, and Pt catalysts: a comparative study of nanoparticles and bulk materials. *ACS Catal.* **2**, 1765–1772 (2012).
16. Mavrokefalos, C. K. & Patzke, G. R. Water oxidation catalysts: the quest for new oxide-based materials. *Inorganics* **7**, 29 (2019).
17. Thorarinsdottir, A. E. & Nocera, D. G. Energy catalysis needs ligands with high oxidative stability. *Chem. Catal.* **1**, 32–43 (2021). Rule sets for the design of stable homogeneous and heterogeneous catalysts under oxidizing environments.
18. Li, J. et al. Molecular and heterogeneous water oxidation catalysts: recent progress and joint perspectives. *Chem. Soc. Rev.* **50**, 2444–2485 (2021).
19. Sapountzi, F. M., Gracia, J. M., Westrate, C. J., Fredriksson, H. O. A. & Niemantsverdriet, J. W. Electrocatalysts for the generation of hydrogen, oxygen and synthesis gas. *Prog. Energy Combust. Sci.* **58**, 1–35 (2017).

20. Lux, H. "Säuren" und "basen" im schmelzfluss: die bestimmung der sauerstoffionen-konzentration. *Ztschr. Elektrochem.* **45**, 303–309 (1939).
21. Esswein, A. J., Surendranath, Y., Reece, S. Y. & Nocera, D. G. Highly active cobalt phosphate and borate based oxygen evolving catalysts operating in neutral and natural waters. *Energy Environ. Sci.* **4**, 499–504 (2011).
22. Steinmiller, E. M. P. & Choi, K.-S. Photochemical deposition of cobalt-based oxygen evolving catalyst on a semiconductor photoanode for solar oxygen production. *Proc. Natl. Acad. Sci. USA* **106**, 20633–20636 (2009).
23. Zhong, D. K., Choi, S. & Gamelin, D. R. Near-complete suppression of surface recombination in solar photoelectrolysis by "Co-Pi" catalyst-modified W:$BiVO_4$. *J. Am. Chem. Soc.* **133**, 18370–18377 (2011).
24. Pijpers, J. J. H., Winkler, M. T., Surendranath, Y., Buonassisi, T. & Nocera, D. G. Light-induced water oxidation at silicon electrodes functionalized with a cobalt oxygen-evolving catalyst. *Proc. Natl. Acad. Sci. USA* **108**, 10056–10061 (2011).
25. Reece, S. Y. et al. Wireless solar water splitting using silicon-based semiconductors and earth-abundant catalysts. *Science* **334**, 645–648 (2011).
26. Nocera, D. G. The artificial leaf. *Acc. Chem. Res.* **45**, 767–776 (2012).
27. Kornienko, N., Zhang, J. Z., Sakimoto, K. K., Yang, P. & Reisner, E. Interfacing nature's catalytic machinery with synthetic materials for semi-artificial photosynthesis. *Nat. Nanotechnol.* **13**, 890–899 (2018).
28. Sherbo, R. S., Loh, D. M. & Nocera, D. G. Hybrid biological-inorganic systems for CO_2 conversion to fuels. In *Carbon Dioxide Electrochemistry: Homogeneous and Heterogeneous Catalysis* (eds Robert, M., Costentin, C. & Daasbjerg, K.) Ch. 8 (Royal Society of Chemistry, 2021).
29. Mohammadi, M. R. et al. Exploring the limits of self-repair in cobalt oxide films for electrocatalytic water oxidation. *ACS Catal.* **10**, 7990–7999 (2020). Definition of self-healing from a structure/composition viewpoint as opposed to operational viewpoint.
30. Costentin, C. & Nocera, D. G. Self-healing catalysis in water. *Proc. Natl. Acad. Sci. USA* **114**, 13380–13384 (2017). Formal kinetics model of self-healing processes.
31. Cremaldi, J. C. & Bhushan, B. Bioinspired self-healing materials: lessons from nature. *Beilstein J. Nanotechnol.* **9**, 907–935 (2018).
32. Speck, O. & Speck, T. An overview of bioinspired and biomimetic self-repairing materials. *Biomimetics* **4**, 26 (2019).
33. Li, G. *Self-Healing Composites: Shape Memory Polymer Based Structures,* 21–34 (John Wiley & Sons, 2014).
34. Blaiszik, B. J. et al. Self-healing polymers and composites. *Annu. Rev. Mater. Res.* **40**, 179–211 (2010).
35. Yang, Y. & Urban, M. W. Self-healing polymeric materials. *Chem. Soc. Rev.* **42**, 7446–7467 (2013).
36. *Self Healing Materials—An Alternative Approach to 20 Centuries of Materials Science* (ed. van der Zwaag, S.) (Springer, 2007).
37. Amendola, V. & Meneghetti, M. Self-healing at the nanoscale. *Nanoscale* **1**, 74–88 (2009).
38. *Self-Healing Materials: Fundamentals, Design Strategies, and Applications* (ed. Ghosh, S. K.) (Wiley-VCH, 2009).
39. Aro, E.-M., Virgin, I. & Andersson, B. Photoinhibition of photosystem II. Inactivation, protein damage and turnover. *Biochim. Biophys. Acta* **1143**, 113–134 (1993).
40. Theis, J. & Schroda, M. Revisiting the photosystem II repair cycle. *Plant Signal. Behav.* **11**, e1218587 (2016).
41. Najafpour, M. M., Khoshkam, M., Sedigh, D. J., Zahraei, A. & Kompany-Zareh, M. Self-healing for nanolayered manganese oxides in the presence of cerium(IV) ammonium nitrate: new findings. *New J. Chem.* **39**, 2547–2550 (2015).
42. Hocking, R. K. et al. Water-oxidation catalysis by manganese in a geochemical-like cycle. *Nat. Chem.* **3**, 461–466 (2011).
43. Zhong, H., Wang, J., Meng, F. & Zhang, X. In situ activating ubiquitous rust towards low-cost, efficient, free-standing, and recoverable oxygen evolution electrodes. *Angew. Chem. Int. Ed.* **55**, 9937–9941 (2016).
44. Najafpour, M. M. et al. Damage management in water-oxidizing catalysts: from photosystem II to nanosized metal oxides. *ACS Catal.* **5**, 1499–1512 (2015).
45. Spöri, C., Kwan, J. T. H., Bonakdarpour, A., Wilkinson, D. P. & Strasser, P. The stability challenges of oxygen evolving catalysts: towards a common fundamental understanding and mitigation of catalyst degradation. *Angew. Chem. Int. Ed.* **56**, 5994–6021 (2017). Overview of various degradation mechanisms of OER catalysts.
46. Kanan, M. W., Surendranath, Y. & Nocera, D. G. Cobalt-phosphate oxygen-evolving compound. *Chem. Soc. Rev.* **38**, 109–114 (2009).
47. Bediako, D. K., Ullman, A. M. & Nocera, D. G. Catalytic oxygen evolution by cobalt oxido thin films. *Top. Curr. Chem.* **371**, 173–213 (2016).
48. Suen, N.-T. et al. Electrocatalysis for the oxygen evolution reaction: recent development and future perspectives. *Chem. Soc. Rev.* **46**, 337–365 (2017).
49. Roger, I., Shipman, M. A. & Symes, M. D. Earth-abundant catalysts for electrochemical and photoelectrochemical water splitting. *Nat. Rev. Chem.* **1**, 0003 (2017).
50. Kanan, M. W. & Nocera, D. G. In situ formation of an oxygen-evolving catalyst in neutral water containing phosphate and Co^{2+}. *Science* **321**, 1072–1075 (2008). Discovery of self-healing OER metal-oxide catalysts.
51. Surendranath, Y., Dincă, M. & Nocera, D. G. Electrolyte-dependent electrosynthesis and activity of cobalt-based water oxidation catalysts. *J. Am. Chem. Soc.* **131**, 2615–2620 (2009).
52. Farrow, C. L., Bediako, D. K., Surendranath, Y., Nocera, D. G. & Billinge, S. J. L. Intermediate-range structure of self-assembled cobalt-based oxygen-evolving catalyst. *J. Am. Chem. Soc.* **135**, 6403–6406 (2013).
53. Du, P., Kokhan, O., Chapman, K. W., Chupas, P. J. & Tiede, D. M. Elucidating the domain structure of the cobalt oxide water splitting catalyst by x-ray pair distribution function analysis. *J. Am. Chem. Soc.* **134**, 11096–11099 (2012).
54. Kanan, M. W. et al. Structure and valency of a cobalt-phosphate water oxidation catalyst determined by in situ x-ray spectroscopy. *J. Am. Chem. Soc.* **132**, 13692–13701 (2010).
55. Kwon, G. et al. Resolution of electronic and structural factors underlying oxygen-evolving performance in amorphous cobalt oxide catalysts. *J. Am. Chem. Soc.* **140**, 10710–10720 (2018).
56. Ullman, A. M., Brodsky, C. N., Li, N., Zheng, S.-L. & Nocera, D. G. Probing edge site reactivity of oxidic cobalt water oxidation catalysts. *J. Am. Chem. Soc.* **138**, 4229–4236 (2016).
57. Bergmann, A. et al. Unified structural motifs of the catalytically active state of Co(oxyhydr)oxides during the electrochemical oxygen evolution reaction. *Nat. Catal.* **1**, 711–719 (2018).
58. Mattioli, G., Giannozzi, P., Amore Bonapasta, A. & Guidoni, L. Reaction pathways for oxygen evolution promoted by cobalt catalyst. *J. Am. Chem. Soc.* **135**, 15353–15363 (2013).
59. Chen, J. & Selloni, A. First principles study of cobalt (hydr)oxides under electrochemical conditions. *J. Phys. Chem. C* **117**, 20002–20006 (2013).
60. Winkler, J. R. & Gray, H. B. Electronic structures of oxo-metal ions. In *Molecular Electronic Structures of Transition Metal Complexes I. Structure and Bonding,* Vol. 142 (eds Mingos, D. M. P., Day, P. & Dahl, J. P.) 17–28 (Springer, 2012).
61. Surendranath, Y., Kanan, M. W. & Nocera, D. G. Mechanistic studies of the oxygen evolution reaction by a cobalt-phosphate catalyst at neutral pH. *J. Am. Chem. Soc.* **132**, 16501–16509 (2010).
62. McAlpin, J. G. et al. EPR evidence for Co(IV) species produced during water oxidation at neutral pH. *J. Am. Chem. Soc.* **132**, 6882–6883 (2010).
63. Risch, M. et al. Water oxidation by amorphous cobalt-based oxides: in situ tracking of redox transitions and mode of catalysis. *Energy Environ. Sci.* **8**, 661–674 (2015).
64. Sisley, M. J. & Jordan, R. B. First hydrolysis constants of hexaaquacobalt(III) and -manganese(III): longstanding issues resolved. *Inorg. Chem.* **45**, 10758–10763 (2006).
65. Surendranath, Y., Lutterman, D. A., Liu, Y. & Nocera, D. G. Nucleation, growth, and repair of a cobalt-based oxygen evolving catalyst. *J. Am. Chem. Soc.* **134**, 6326–6336 (2012).
66. Symes, M. D., Surendranath, Y., Lutterman, D. A. & Nocera, D. G. Bidirectional and unidirectional PCET in a molecular model of a cobalt-based oxygen-evolving catalyst. *J. Am. Chem. Soc.* **133**, 5174–5177 (2011).
67. Costentin, C. & Nocera, D. G. Dual-phase molecular-like charge transport in nanoporous transition metal oxides. *J. Phys. Chem. C* **123**, 1966–1973 (2019).
68. Lutterman, D. A., Surendranath, Y. & Nocera, D. G. A self-healing oxygen-evolving catalyst. *J. Am. Chem. Soc.* **131**, 3838–3839 (2009).
69. Han, A., Wu, H., Sun, Z., Jia, H. & Du, P. Facile deposition of nanostructured cobalt oxide catalysts from molecular cobaloximes for efficient water oxidation. *Phys. Chem. Chem. Phys.* **15**, 12534–12538 (2013).
70. Gerken, J. B., Landis, E. C., Hamers, R. J. & Stahl, S. S. Fluoride-modulated cobalt catalysts for electrochemical oxidation of water under non-alkaline conditions. *ChemSusChem* **3**, 1176–1179 (2010).
71. Gerken, J. B. et al. Electrochemical water oxidation with cobalt-based electrocatalysts from pH 0–14; the thermodynamic basis for catalyst structure, stability, and activity. *J. Am. Chem. Soc.* **133**, 14431–14442 (2011).
72. Bloor, L. G., Molina, P. I., Symes, M. D. & Cronin, L. Low pH electrolytic water splitting using earth-abundant metastable catalysts that self-assemble in situ. *J. Am. Chem. Soc.* **136**, 3304–3311 (2014).
73. Huynh, M., Bediako, D. K., Liu, Y. & Nocera, D. G. Nucleation and growth mechanisms of an electrodeposited manganese oxide oxygen evolution catalyst. *J. Phys. Chem. C* **118**, 17142–17152 (2014).
74. Huynh, M., Bediako, D. K. & Nocera, D. G. A functionally stable manganese oxide oxygen evolution catalyst in acid. *J. Am. Chem. Soc.* **136**, 6002–6010 (2014).
75. Huynh, M., Shi, C., Billinge, S. J. L. & Nocera, D. G. Nature of activated manganese oxide for oxygen evolution. *J. Am. Chem. Soc.* **137**, 14887–14904 (2015).
76. Pourbaix, M. *Atlas of Electrochemical Equilibria in Aqueous Solutions* (National Association of Corrosion Engineers, 1974).
77. Zaharieva, I. et al. Electrosynthesis, functional, and structural characterization of a water-oxidizing manganese oxide. *Energy Environ. Sci.* **5**, 7081–7089 (2012).

78. Dincă, M., Surendranath, Y. & Nocera, D. G. A nickel-borate oxygen-evolving catalyst that functions under benign conditions. *Proc. Natl. Acad. Sci. USA* **107**, 10337–10341 (2010).
79. Bediako, D. K., Surendranath, Y. & Nocera, D. G. Mechanistic studies of the oxygen evolution reaction mediated by a nickel–borate thin film electrocatalyst. *J. Am. Chem. Soc.* **135**, 3662–3674 (2013).
80. Bediako, D. K. et al. Structure–activity correlations in a nickel–borate oxygen evolution catalyst. *J. Am. Chem. Soc.* **134**, 6801–6809 (2012).
81. Singh, A., Chang, S. L. Y., Hocking, R. K., Bach, U. & Spiccia, L. Highly active nickel oxide water oxidation catalysts deposited from molecular complexes. *Energy Environ. Sci.* **6**, 579–586 (2013).
82. Du, J., Chen, Z., Ye, S., Wiley, B. J. & Meyer, T. J. Copper as a robust and transparent electrocatalyst for water oxidation. *Angew. Chem. Int. Ed.* **54**, 2073–2078 (2015).
83. Huynh, M., Ozel, T., Liu, C., Lau, E. C. & Nocera, D. G. Design of template-stabilized active and earth-abundant oxygen evolution catalysts in acid. *Chem. Sci.* **8**, 4779–4794 (2017).
84. Li, N. et al. Template-stabilized oxidic nickel oxygen evolution catalysts. *Proc. Natl. Acad. Sci. USA* **117**, 16187–16192 (2020).
85. Chatti, M. et al. Intrinsically stable in situ generated electrocatalyst for long-term oxidation of acidic water at up to 80 °C. *Nat. Catal.* **2**, 457–465 (2019).
86. Trotochaud, L., Ranney, J. K., Williams, K. N. & Boettcher, S. W. Solution-cast metal oxide thin film electrocatalysts for oxygen evolution. *J. Am. Chem. Soc.* **134**, 17253–17261 (2012).
87. Trotochaud, L., Young, S. L., Ranney, J. K. & Boettcher, S. W. Nickel–iron oxyhydroxide oxygen-evolution electrocatalysts: the role of intentional and incidental iron incorporation. *J. Am. Chem. Soc.* **136**, 6744–6753 (2014).
88. Swierk, J. R., Klaus, S., Trotochaud, L., Bell, A. T. & Tilley, T. D. Electrochemical study of the energetics of the oxygen evolution reaction at nickel iron (oxy) hydroxide catalysts. *J. Chem. Phys. C* **119**, 19022–19029 (2015).
89. Li, N., Hadt, R. G., Hayes, D., Chen, L. X. & Nocera, D. G. Detection of high-valent iron species in alloyed oxidic cobaltates for catalysing the oxygen evolution reaction. *Nat. Commun.* **12**, 4218 (2021).
90. Görlin, M. et al. Oxygen evolution reaction dynamics, faradaic charge efficiency, and the active metal redox states of Ni−Fe oxide water splitting electrocatalysts. *J. Am. Chem. Soc.* **138**, 5603–5614 (2016).
91. Shin, H., Xiao, H. & Goddard, W. A. III. In silico discovery of new dopants for Fe-doped Ni oxyhydroxide ($Ni_{1-x}Fe_xOOH$) catalysts for oxygen evolution reaction. *J. Am. Chem. Soc.* **140**, 6745–6748 (2018).
92. Li, N. et al. Influence of iron doping on tetravalent nickel content in catalytic oxygen evolving films. *Proc. Natl. Acad. Sci. USA* **114**, 1486–1491 (2017).
93. Zou, S. et al. Fe (oxy)hydroxide oxygen evolution reaction electrocatalysis: intrinsic activity and the roles of electrical conductivity, substrate, and dissolution. *Chem. Mater.* **27**, 8011–8020 (2015).
94. Yang, M. et al. Fe(Co)OOH dynamically stable interface based on self-sacrificial reconstruction for long-term electrochemical water oxidation. *ACS Appl. Mater. Interfaces* **13**, 17450–17458 (2021).
95. Chung, D. Y. et al. Dynamic stability of active sites in hydr(oxy) oxides for the oxygen evolution reaction. *Nat. Energy* **5**, 222–230 (2020).
96. Feng, C. et al. A self-healing catalyst for electrocatalytic and photoelectrochemical oxygen evolution in highly alkaline conditions. *Nat. Commun.* **12**, 5980 (2021).
97. Wang, J., Ji, L. & Chen, Z. In situ rapid formation of a nickel–iron-based electrocatalyst for water oxidation. *ACS Catal.* **6**, 6987–6992 (2016).
98. Kuang, Y. et al. Ultrastable low-bias water splitting photoanodes via photocorrosion inhibition and in situ catalyst regeneration. *Nat. Energy* **2**, 16191 (2016).
99. Boddula, R. et al. Synergetic effects of dual electrocatalysts for high-performance solar-driven water oxidation. *ACS Appl. Energy Mater.* **2**, 7256–7262 (2019).
100. Barwe, S. et al. Overcoming the instability of nanoparticle-based catalyst films in alkaline electrolyzers by using self-assembling and self-healing films. *Angew. Chem. Int. Ed.* **56**, 8573–8577 (2017).
101. Xiao, M. et al. Regenerable catalyst for highly alkaline water oxidation. *ACS Energy Lett.* **6**, 1677–1683 (2021).
102. Tahini, H. A., Tan, X., Schwingenschlögl, U. & Smith, S. C. In operando self-healing of perovskite electrocatalysts: a case study of $SrCoO_3$ for the oxygen evolution reaction. *Part. Part. Syst. Charact.* **34**, 1600280 (2017).
103. Zhang, Y. et al. Direct observation of oxygen vacancy self-healing on TiO_2 photocatalysts for solar water splitting. *Angew. Chem. Int. Ed.* **58**, 14229–14233 (2019).
104. Ganesan, K. & Murugan, P. First principles calculations on oxygen vacant hydrated α-MnO_2 for activating water oxidation and its self-healing mechanism. *Phys. Chem. Chem. Phys.* **18**, 22196–22202 (2016).
105. Cox, C. R., Lee, J. Z., Nocera, D. G. & Buonassisi, T. Ten-percent solar-to-fuel conversion with nonprecious materials. *Proc. Natl. Acad. Sci. USA* **111**, 14057–14061 (2014).

Acknowledgements

Material is based upon work supported under the Solar Photochemistry Program of the Chemical Sciences, Geosciences and Biosciences Division, Office of Basic Energy Sciences of the U.S. Department of Energy DE-SC0017619. A.E.T. acknowledges the Harvard University Center for the Environment (HUCE) for a postdoctoral fellowship and S.V.V. acknowledges support from the Herchel Smith Graduate Fellowship in the Sciences.

Author contributions

D.G.N. developed the idea and supervised the work. A.E.T. and S.S.V. organized content and designed figures. All authors contributed to the writing of the manuscript.

Competing interests

The authors declare no competing interests.

Additional information

Correspondence and requests for materials should be addressed to Daniel G. Nocera.

Reprints and permission information is available at http://www.nature.com/reprints

Publisher's note Springer Nature remains neutral with regard to jurisdictional claims in published maps and institutional affiliations.